Applied Thermal Engineering 31 (2011) 3542–3551

Contents lists available at ScienceDirect

Applied Thermal Engineering

journal homepage: www.elsevier.com/locate/apthermeng

Performance improvements in low side scroll compressor with extended operation speeds

Yuehju Tang [a,b], Chinghua Hung [a,*], Yuchoung Chang [b]

[a] Department of Mechanical Engineering, National Chiao Tung University, EE452, 1001 Ta Hsueh Road, Hsinchu 300, Taiwan
[b] Green Energy & Environment Research Laboratories, Industrial Technology Research Institute, Taiwan

ARTICLE INFO

Article history:
Received 31 January 2011
Accepted 8 July 2011
Available online 18 July 2011

Keywords:
Axial-compliant mechanism
Suspension structure
Scroll compressor
Inner leakage
Extended operation speed

ABSTRACT

Scroll-type compressors (STCs) are widely used in modern air conditioners for higher efficiency and durability. However, the internal leakage, caused during un-rating operated speed, reduces the volumetric efficiency and influences the performance of STCs. This paper has proposed an axial-compliant mechanism (ACM), composed of a suspension structure and a limiting ring, to solve the leakage problem of a low side STC running in extended speeds. The aim of this ACM design is to control the leakage by keeping optimum clearance. By integrating the verified STC performance simulation package with the internal leakage model, the optimum clearance between scroll tip and bottom plate has been investigated. After the numerical simulation, by employing suitable designs, an improved ACM prototype has been developed and tested. The experimental results show that low leakage, noise, and power consumption are achieved during compression processes even with extended operation speeds, and moreover, the overall coefficient of performance is increased from 0.61% to 13.53%. In this study, the proposed design is useful for enhancing the performance of low side type STCs.

1. Introduction

The scroll-type compressor (STC) is an important component in modern air conditioner devices because of its high efficiency, low noise, simple mechanism, and high reliability. Further, in recent years, researches on STCs have primarily focused on enhancing their performance by employing new technologies. For example, one such technology—the variable speed control (or, inverter-fed drive)—can improve the efficiency and reduce energy consumption [1–3] However, to construct a variable speed scroll compressor prototype is very expensive and unrealistic. Therefore, many researchers have employed numerical methods for STC performance investigation. Most of these numerical methods can be classified into two categories: “dynamic analysis of compliances” and “thermodynamic analysis of scroll operations”. In addition to this, the STC design theories and its geometric aspects have been reported previously [4,5]. Further investigations, about the variations in the compressor performance when a self-adjusting back-pressure mechanism is employed for axial compliance, have been conducted [6]. A suction process using a dynamic model also has been analyzed [7]. The losses resulting from friction, compression, and leakage have also been studied with numerical analyses and experiments [8].

Most of these studies indicated that the friction losses were due to the contact behavior whereas the leakage losses were a result of the type of sealing between the orbiting and fixed scrolls. Since the internal leakages not only decrease the cooling capacity but also influence the balancing of inner forces, especially at extended, i.e., both higher and lower, operation speeds. Therefore, it is extremely important to solve the leakage problem to ensure reliability and energy saving.

The above studies have also suggested that the best method to reduce internal leakage is to control the balance of internal forces of the compressor using a compliant mechanism, and this will help to maintain an optimal clearance between the scroll warps. However, in the previous results, they have pointed out the compliant mechanism is quite different in high-pressure shell (HPS) STC and low pressure shell (LPS) STC. Both these STC types have extremely different method for controlling the optimum scroll clearance due to the differences in the characteristics of the pressure difference [9–11].

The previous literatures have also reported investigations about the leakage characteristics in STCs such as, leakage mass flow rate, leakage model, experimental investigations, and computer fluid simulations. However, few researches have been conducted on robust ACM designs for achieving energy savings on an LPS STC operating at extended operation speeds.

* Corresponding author. Tel.: +886 3 5712121x55160; fax: +886 3 5720634.
E-mail addresses: JoshYJTang@itri.org.tw (Y. Tang), chhung@mail.nctu.edu.tw (C. Hung).

1359-4311/$ – see front matter
doi:10.1016/j.applthermaleng.2011.07.009

Nomenclatures

L	length of leakage path (mm)
l	scroll warp thickness (mm)
M	mass (kg)
p	pressure (MPa)
p_1	pressure at optimum rating (MPa)
p_2	pressure at initial rating (MPa)
p_d	discharge pressure (MPa)
p_i,p_o	inner pressure (MPa); outer pressure (MPa)
r_i, r_o	leakage path inner radius (mm); leakage path outer radius (mm)
r_m	leakage path mean radius (mm)
T,t	Temperature (°C); time (second)
u	velocity (mm/s)
X	spring deformation distance (mm)
y	length of y direction (mm)

Greek letters

δ	scroll radial gap (μm)
μ_{mn}	coefficient of dynamic viscosity (Pa s)
υ	kinematic viscosity (m^2/s)
ρ	density (kg/m^3)
ρ_{mn}	mean density (kg/m^3)
τ	shearing force (Nt)

In this paper, a simple leakage model is constructed by transforming the involute leakage path into a circular path and integrated into a previously developed STC performance simulation package (ITRI_STC) [12]. Further, this paper have constructed a pulse-width-modulated (PWM) inverter and scroll compressor prototype using the proposed ACM and characterized the STC experimentally. The energy savings will also been verified by experimental tests using our variable speed STC prototype. The research results may help to improve the significant performance with extended operation speeds.

2. Numerical simulations of leakage effect of STC

The leakage flows have been analyzed previously with various models [13–18]. In these studies, not only theoretical investigations but also experimental investigations have been conducted for the analysis of leakage parameters [13–15]. These researches demonstrated that the radial leakage (also called tip leakage) is more critical than the flank leakage because the leakage path is considerably longer. (Fig. 1) In this study, the radial leakage problems have been investigated. The results contributed to enhance the ACM design performance at extended operation speeds.

2.1. Modeling radial leakage

Most of the commercially available designs (such as floating tip seals [18]) are usually applied to reduce radial leakages and to prevent friction losses in the STCs. However, this increases the manufacturing costs and requires precise assembly works. Furthermore, lower operating speed and lower pressure different make the floating tip seal fail. Therefore, the designs with no floating tip seals for compressor effectively raising by reducing radial leakage are using by modern scroll compressor manufactures such as Copeland, Hitachi, Matsushita and so on. In such designs, the radial leakage path can be considered as a circular (Fig. 2). The radial leakage is calculated by introducing one-dimensional flat plate flow (Fig. 3). The direct leakage path is the scroll warp thickness (can be considered as a constant value). Although the leakage path direction

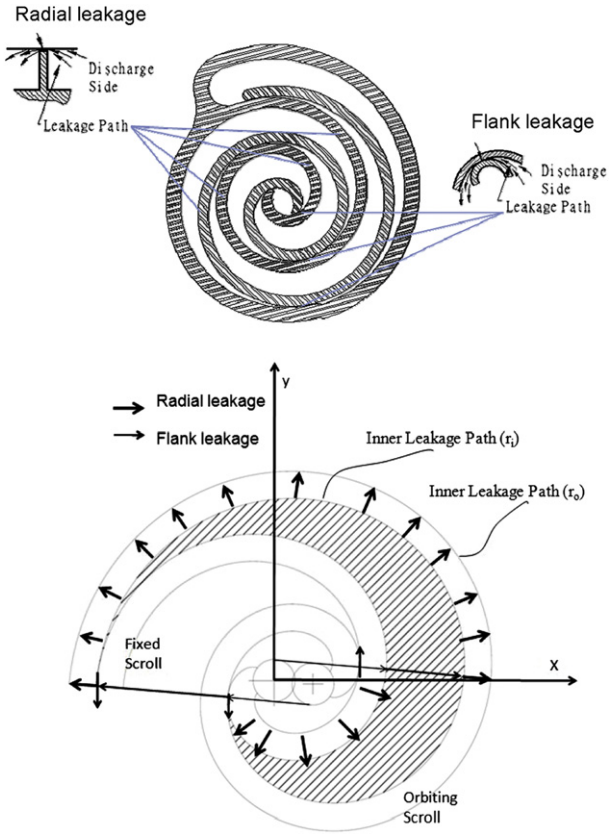

Fig. 1. Involute leakage path.

along the scroll curve changes with the orbiting angle, the typical path can be projected as several concentric circles, and the simplified leakage path is similar to the ring-type leakage path. (Fig. 4).

We have employed the following assumptions in this leakage model in order to simplify the numerical analysis:

(a) The leakage along the y direction is extremely low, as shown in Fig. 3, and can be considered to be related only to the pressure, temperature, and mean fluid density, depending on the x direction.

$$P = P(x); T = T(x); \rho_{mn} = \rho_{mn}(x) \tag{1}$$

(b) The fluid is a mixture of refrigerant and oil, and can be regarded as a Newtonian fluid.

$$\tau = \mu_{mn}\frac{\partial u}{\partial y} \tag{2}$$

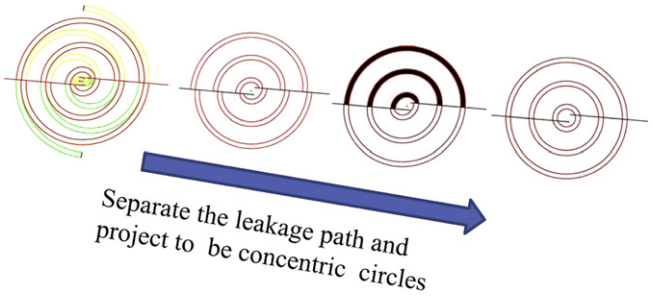

Fig. 2. Integrated the simplified leakage path model (as circle path).

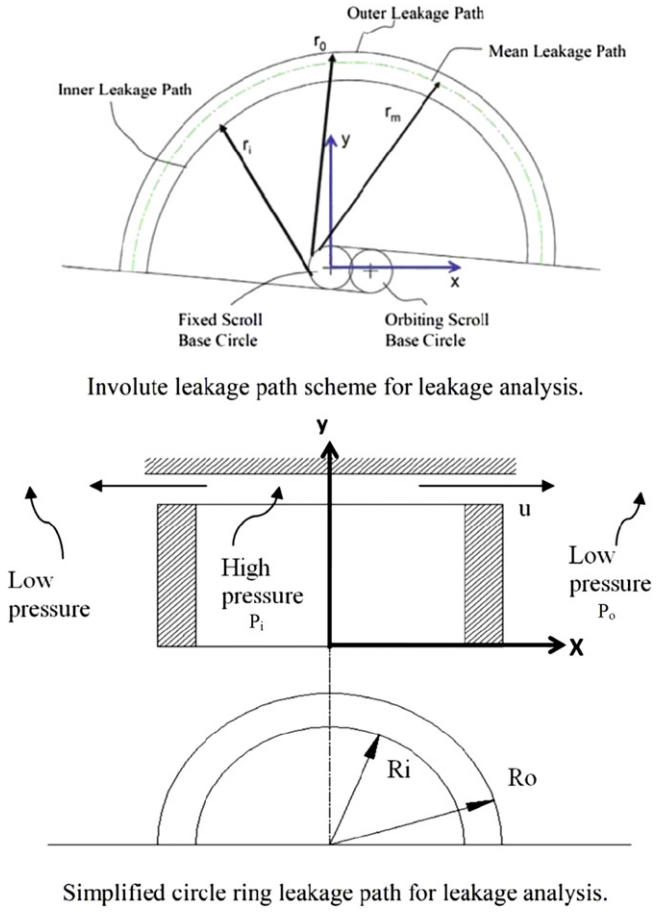

Fig. 3. Leakage flow simulation model.

(c) For small clearances, the flow direction can be regarded as one-dimensional; moreover, the velocity in the y direction is considered to be zero.

When the clearance (δ) is very small, the fluid flow direction can be regarded as one-dimensional flow; this implies that the flow velocity in the y direction can be considered as zero. ($v = 0$). From the assumptions (a) and (c), the continuity equation is

$$\frac{\partial u}{\partial x} = 0 \tag{3}$$

Thus, the flow velocity is a function of y as follows:

$$u = u(y) \tag{4}$$

The momentum equation of the leakage flow is

$$-\frac{\partial p}{\partial x} + \mu_{mn}\left(\frac{\partial^2 u}{\partial y^2}\right) = \rho_{mn}\left(u\frac{\partial u}{\partial x} + v\frac{\partial u}{\partial y}\right) \tag{5}$$

From the above conditions, equation (5) can be expressed as

$$\frac{\partial^2 u}{\partial y^2} = \frac{1}{\mu_{mn}}\frac{dp}{dx} \tag{5a}$$

The variables p, dp/dr, and μ_{mn} are independent of y, and equation (5a) can be integrated with respect to y under the boundary conditions

$$\begin{aligned} u(y = 0) &= 0 \\ u(y = \delta) &= 0 \end{aligned} \tag{6}$$

If the boundary conditions are substituted into equation (5a), the velocity distribution of the leakage depends only on the clearance as follows:

$$u = -\frac{y}{2\mu_{mn}}(\delta - y)\frac{dp}{dx} \tag{7}$$

Hence, the leakage mass flow rate (dM/dt) is

$$\frac{dM}{dt} = L\int_0^{\delta} \rho u dy = -\frac{1}{2}L\rho_{mn}\left(\frac{\delta^3}{6\mu_{mn}}\frac{dp}{dx}\right) \tag{8}$$

The pressure gradient in the leakage channel is considered to be a linear distribution along the x direction; it is

$$\frac{dp}{dx} = \frac{p_i - p_o}{l}.$$

The mass flow rate of the radial leakage can be calculated by

$$\frac{dM}{dt} = L\rho_{mn}\left(\frac{\delta^3(p_i - p_o)}{12\mu_{mn}l}\right) \tag{9}$$

This equation has several explanations as follows:

(1) $dM/dt = \infty L$; This shows that the shorter the sealed length, greater the volumetric efficiency.
(2) The leakage mass is proportional to the scroll gap (δ).
(3) The leakage direction is identical to the pressure difference direction, and the mass leakage increases with the pressure difference.
(4) Leakage decreases as the coefficient of dynamic viscosity (μ_{mn}) increases.
(5) Since the leakage direction is opposite to the velocity direction, as the compressor speed increases, leakage decreases.

By introducing the ring leakage model of the rolling piston pump [19], the leakage model is based on several half-ring leakage paths that are equivalent to the original involute leakage path (Fig. 4). The scroll warp thickness (l) is equivalent to the mean radius ± half warp thickness ($l/2$), while the mean radius (r_m) is $L/2\pi$ (Fig. 3).

Finally, the radial leakage model in the form of polar coordinates is

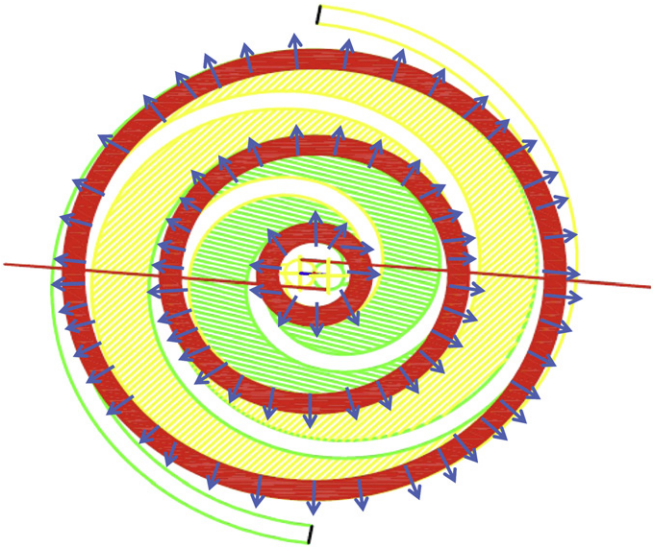

Fig. 4. Concentric circles as leakage path.

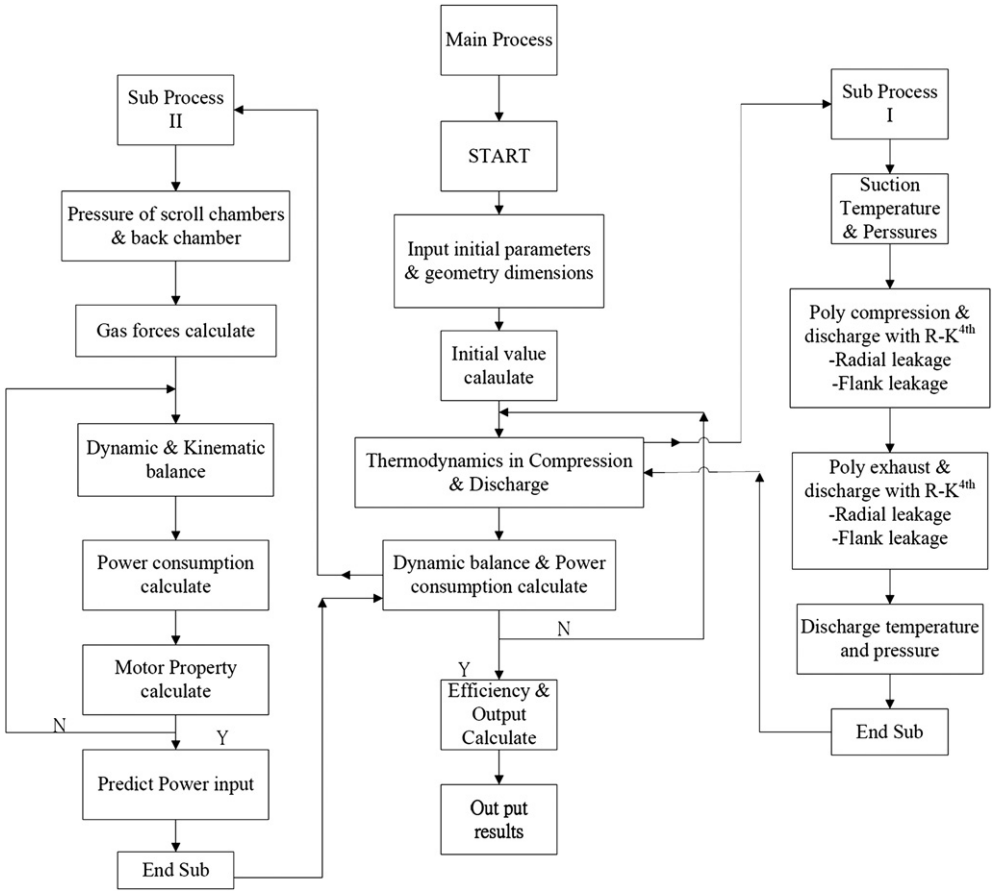

Fig. 5. The calculate algorithm of leakage.

$$\frac{dM}{dt} = \frac{\pi\delta^3(p_i - p_o)}{6\upsilon \ln\left(\frac{r_o}{r_i}\right)} \tag{10}$$

In equation (10), υ is an average value because it depends on the oil mass percentage of the leakage fluid [19].

Table 1
STC Parameters and experiment operating conditions.

Parameters of the LPS STC		
Parameters		Value
Radius of the basic circle of the scroll(a)(mm)		2.062
Thickness of the scroll(t)(mm)		2.65
Involutes angle of the scroll(φi)(degree)		1150
scroll pitch(Tp)(mm)		12.956
scroll wrap height(hs)(mm)		25.2
Experiment operating conditions		
Environment conditions		Value
Condensing temperature(°C)		54.4
Evaporator temperature(°C)		7.2
Superheat(K)		10
Subcool(K)		8.3
Expansion valve temperature(°C)		46.1
Refrigerant		R22
STC operation speed		
Condition	Frequency setting(Hz)	Actual revolution(rpm)
A	40	2261
B	50	2871
C	60	3454
D	70	4033
E	80	4612

2.2. Theoretical performance simulations of clearance influence

In order to investigate the effects of radial leakages on the LSP STC, we have performed simulations of certain case studies using a simulation package [12] combined with REFPROP 8 [20] and the C++ programming language. Fig. 5 presents the calculation algorithm.

Table 2
Compressor prototype and STC performance measurement specification.

Compressor prototype specification		
Compressor characteristics		
Theoretical swept volume @ 60 Hz	7.5762 m3/h	
Nominal speed	3450 rpm	
Maximum operating current	19.2 A	
Usual operating range		
Supply temperature:	18–25 °C	
Exhaust temperature	80–120 °C	
Supply pressure	0.3–0.7 MPa	
Refrigerant mass flow rate	87–290 kg/h	
Electrical power	0.8–3.7 kW	
STC performance measurement specification		
Refrigerant	R22	
Range of cooling capacity	1.5 kW–15 kW	
Test standard- Capacity, COP and volumetric efficiency determination	ASHRAE 23 and ISO 917	
Parameter	Range	Stability
Discharge pressure(MPa)	0.62–3.2	±0.01
Suction pressure(MPa)	0.12–0.96	±0.015
Inlet temperature(°C)	15–52	±0.1
Suction temperature(°C)	−25–38	±0.1
Ambient temperature(°C)	32	±2
Compressor speed(rpm)	1200–7200	± 0.25%

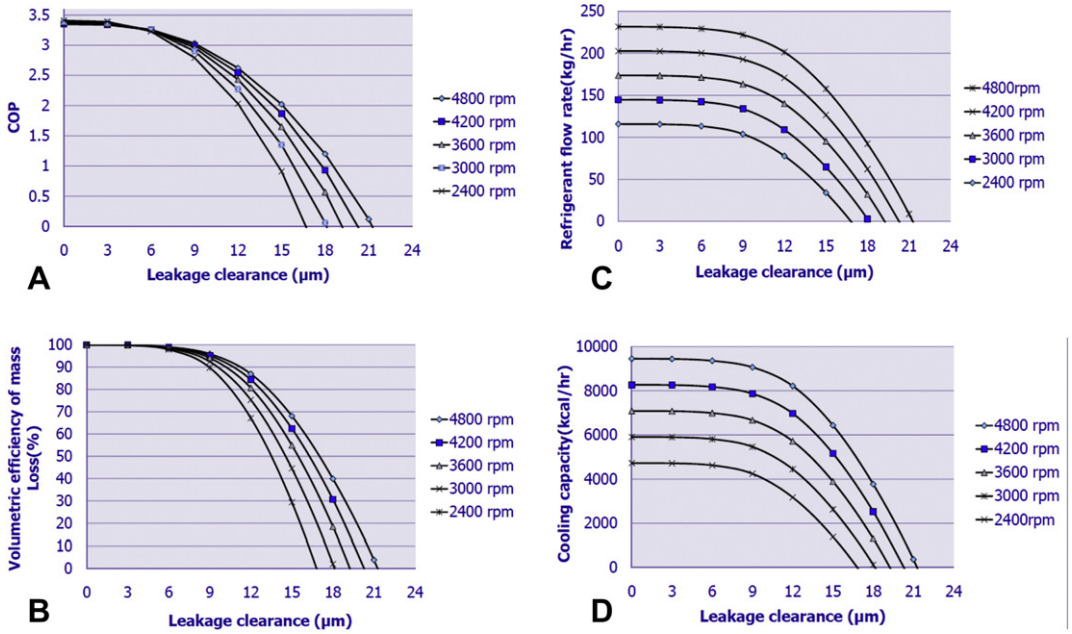

Fig. 6. The calculate result: (A) COP value vs. Leakage clearance; (B) COP value vs. Leakage clearance;(C) Refrigerant flow rate vs. Leakage clearance; (D) Cooling Capacity vs. Leakage clearance.

The following three main definitions of efficiency are employed for evaluating the STC performance:

(a) Coefficient of performance (COP)—the energy proportional to the cooling capacity and compressor electric power consumption;
(b) Volumetric efficiency of leakage gas mass loss—the percentage ratio of actual mass flow rate (i.e. discharge mass flow rate with leakage) to the theoretical discharge mass flow rate;
(c) Isentropic compression efficiency—the ratios of the ideal isentropic compression work to the actual compression work (i.e. motor electric power consumption).

In this study, the main scroll geometric parameters of the LPS STC are listed in Table 1, and the compressor's operating conditions are also listed in Table 1. In order to eliminate the flank leakage influence, the flank clearance was set to be zero during the numerical calculations. Fig. 6 shows the simulation results; here,

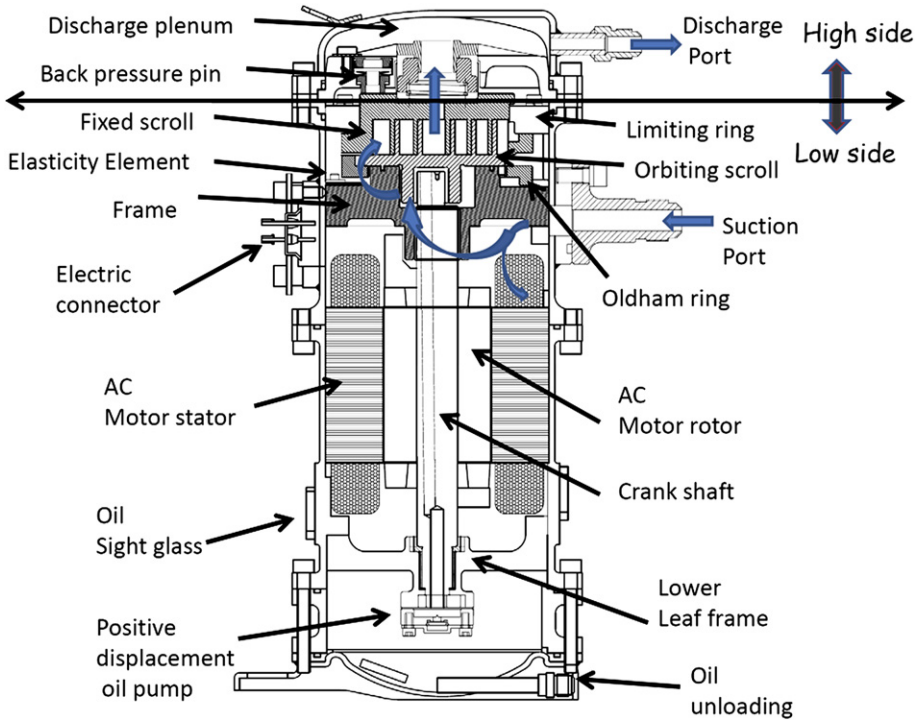

Fig. 7. Scroll compressor prototype profile.

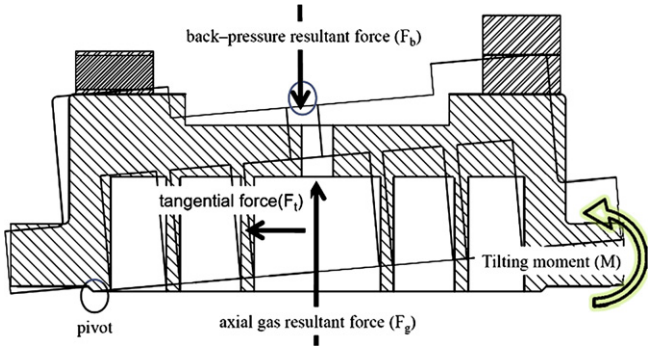

Fig. 8. Diagrammatic sketch of fixed scroll tilting motion and forces.

the scroll clearance (δ) was varied from 0 to 21 μm while the compressor operation frequency were varied from 40 Hz to 80 Hz.

Fig. 6 (A) shows that the COP decreases as the clearance increases, while Fig. 6 (B) shows a similar decrease for the volumetric efficiency of the refrigerant mass loss decreases. Fig. 6(C) and (D) show the refrigerant flow rate and cooling capacity, respectively. From a comparison of these results, the radial clearance should be controlled within 6 μm in order to maintain a high performance of the STC. These results also help to promote better ACM designs and performances.

3. Axial-compliant mechanism (ACM) design

A cross-sectional diagram of the designed LPS STC is shown in Fig. 7. A scroll pump sucks the suction gas, compresses it, and then

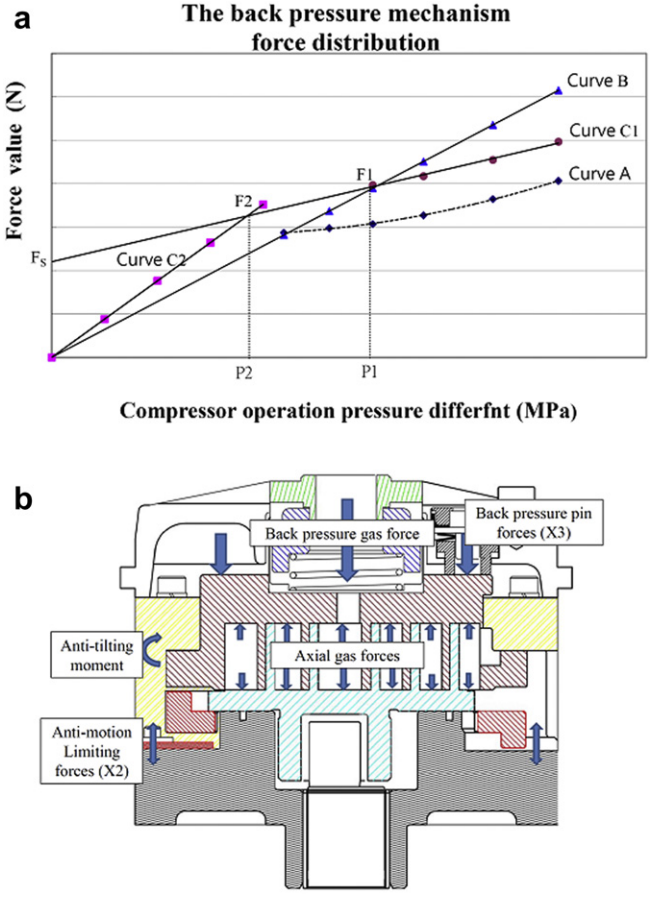

Fig. 9. Force resultant: (a) Forces diagram under variable operation pressure different @ rating (b) Forces balance diagram.

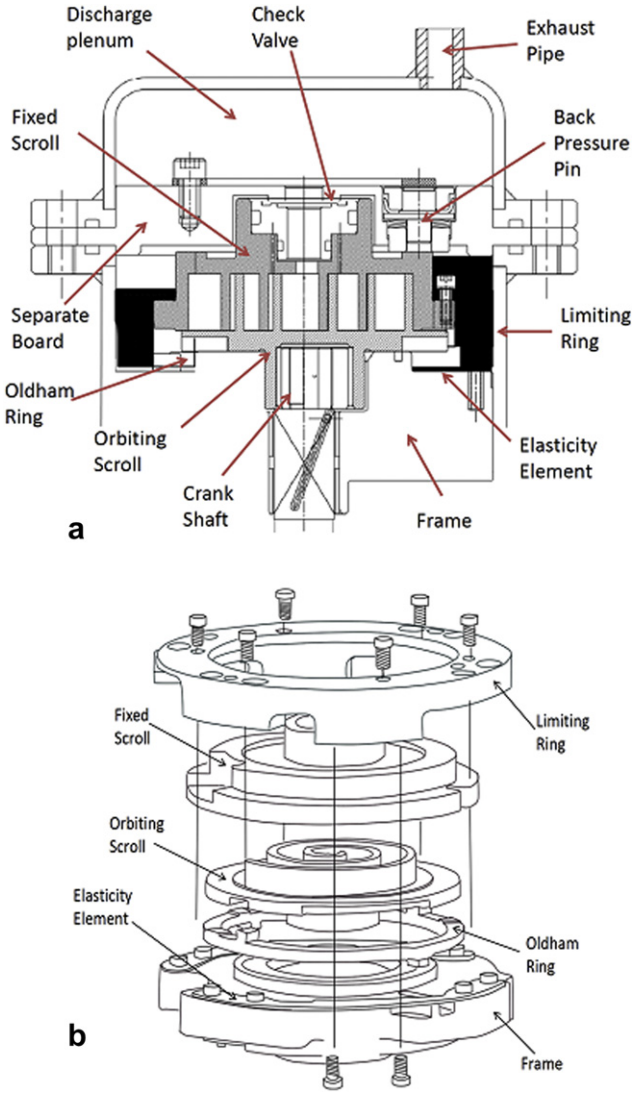

Fig. 10. The suspension compliant mechanism concept: (a) The diagrammatic sketch of the suspension compliant mechanism. (b) The exploded view of the suspension compliant mechanism.

discharges it at high-pressure to the plenum (high side); the exhaust is then emitted out of the discharge port. During the compression process, the orbiting scroll continues to move with a wobble due to the inner unbalanced forces and tilting moments; moreover, the reaction forces and moments make the fixed scroll to wobble as well. Therefore, in order to avoid the occurrence of clearances due to the wobble phenomenon, in this study, the fixed scroll was pressed by

Table 3
Separate forces of fixed scroll at variable compressor operation conditions (For back-pressure mechanism design I).

Condenser temperature (°C)	gas force in scroll chambers (N)	force of the low pressure area (N)	Scroll separating force (N)
45.0	5571.61	2702.22	2869.39
50.0	5618.82	2702.22	2916.60
54.4	5711.98	2702.22	3009.76
60.0	5892.62	2702.22	3189.80
65.0	6236.24	2702.22	3534.02
70.0	6634.59	2702.22	3932.37

(1) Evaporator temperature @ 7.2 °C.
(2) Superheat is10 K and subcool is 8.3 K.
(3) All values are calculated by ITRI STC simulation package.

Table 4
Back-pressure mechanism forces simulation results. (For back-pressure mechanism design II).

Condition	Condenser temperature (°C)	High-pressure (MPa)	Low pressure (MPa)	Pressure difference (MPa)	Pin force (N)	Boss force (N)
a	45.00	1.729	0.625	1.104	368.43	1657.72
b	50.00	1.943	0.625	1.318	440.35	1981.34
c	54.40	2.146	0.625	1.521	509.33	2291.81
d	60.00	2.428	0.625	1.803	589.87	2654.07
e	65.00	2.701	0.625	2.076	699.96	3149.41
f	70.00	2.997	0.625	2.372	803.98	3617.38

(1) Low pressure is the saturation pressure of the evaporator temperature @7.2 °C.
(2) All pressures on the table are "absolute pressure".
(3) All values are calculated by NIST REFPROP 8.0.

a back-pressure mechanism to trace the orbiting scroll in the vertical direction and the orbiting scroll was enforced (by the compressed gas pressure) to keep the orbiting scroll base plate close to the surface of the trust bearing. However, the tangential gas forces make the fixed scroll to be wobbled (Fig. 8).

In the following sub-sections, the back-pressure mechanism and suspension ACM designs for limiting the scroll wobble and controlling the radial clearance near the optimum value (within 6 μm) are described.

3.1. Back-pressure mechanism design

When considering the behavior of LPS STCs during variable speed operations, the most important factor is the variations in the pressure difference between high side and low side in the STC. This causes significant back-pressure changes during the compressor operation and leads to the following two shortcomings:

(1) When the compressor operates at low condensation temperatures or at low pressure differences, the back-pressure decreases leading to poor sealing between the two scrolls and hence leakage. Moreover, in serious situations, due to the leakage, the compressor cannot build up the pressure difference.
(2) The previous scenario reverses when the compressor operates at high condensation temperatures or at high-pressure differences. Excessive back-pressure increases the contact at the two scrolls and makes more friction loss on the interface of the orbiting scroll base plate to the thrust bearing. This will drastically increase the compressor power consumption.

The self-adjusting robust back-pressure mechanism design is as shown in Fig. 9 (a), the curve A represents the net force that can push and separate the two scrolls (this force is called the scroll separation force, and only its maximum value is considered.). Curve

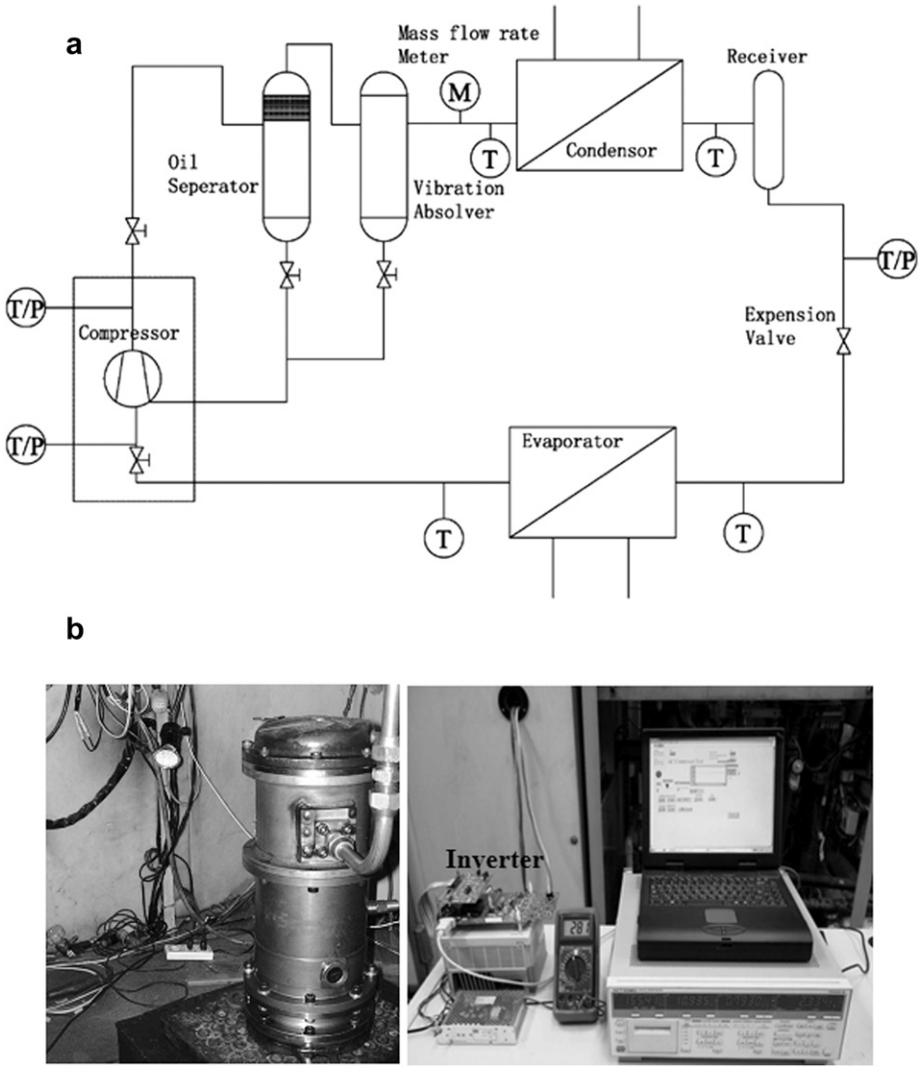

Fig. 11. Test rig scheme & experiment setup: (a) Measurement scheme (b) Prototype for variable speed experiment.

B represents the sum of the back-pressure force and three pressure-pin forces due to the discharge pressure, as shown in Fig. 9 (b). However, curve B can only satisfy the back-pressure during the rating operations. When the STC is operating at un-rating speeds, the pressure difference either decreases or increases, while the back-pressure correspondingly decreases or increases, respectively. Further, at low back-pressures, the leakage loss increases, whereas, at high back-pressures, the friction loss increases.

For providing an optimum back-pressure, the back-pressure force and three pressure-pin forces should have a self-adjusting mechanism. (Fig. 9 (b)) Therefore, the optimum back-pressure distribution curve should be curves C1 and curve C2 that provide a suitable and sufficient back-pressure during any operation conditions. (The curve C1 is construction with the back-pressure force and three pressure-pin forces and disk spring forces. The curve C2 is construction only with the back-pressure force and three pressure-pin forces.) The designing points at P1 and P2 can be used to determine the pushing forces F1 and F2, respectively. Further, using the relationship between force and pressure, the back-pressure areas can be determined by the calculations.

3.2. Suspension ACM design

In this study, an ACM design has been developed to fine-tune the axial motion of the fixed scroll. Fig. 10 shows the suspension ACM; Fig. 10 (a) is the cross-section while Fig. 10 (b) is a magnified explosion view. The design process of the elastic element (two crescent leaf springs) has been verified in detail by Tang et al. [21]; in their study, a design process was formulated to determine the design parameters of the elastic element, and it was verified experimentally. Their results only demonstrate that the ACM can assist the compressor during operations at lower operation speeds from 50 Hz to 34 Hz under the rating conditions. Tables 3 and 4 show the calculation results of the inner forces for designing the back-pressure and suspension ACMs, respectively.

The tilting motion of the fixed scroll due to the tangential gas forces acted at half the height of the fixed scroll warp (Fig. 8). As shown in Fig. 9 (b), the limiting parts provided an anti-moment to overcome the tilting moment, which led to a decrease in the contact noise and leakage caused by the tilting.

In this paper, the ACM prototype has been constructed with the above mechanisms.

4. Experimental setup

In order to verify the compliance prototype, the developed STC was tested using a custom-built PWM inverter placed in a compressor test load stand. As shown in Fig. 11, the test load stand consists of three major parts: a control system, an arrangement of water cooling/heating refrigeration system to maintain fixed suction and charge conditions, and a testing chamber to maintain a constant environment temperature.

The test bench is operated using a classical refrigeration cycle with three main components: a water-heated evaporator, a water-cooled condenser, and an electronic expansion valve. An oil separator system was constructed to ensure the accuracy of the refrigerant mass flow meter.

The STC performance was measured under ASHRAE-T conditions [22] by varying the operation speed from 40 Hz to 80 Hz (Table 1). A control system was used to maintain the specified suction pressure and temperature. The cooling capacity was determined by the refrigerant mass flow rate, compressor speed, and the gas density of the suction refrigerant.

In the study case, the condenser and evaporator temperatures were maintained constant by automatically adjusting the inlet/outlet water flow rate in the heat exchangers using a proportional-integral-derivative (PID) controller. The uncertainty in the refrigerant flow rate is estimated to ±1% of the measured value.

The specifications of the load stand and STC prototype (test sample) are listed in Table 2. The controlled operation conditions and test method (test standard) are also listed in Table 2. The tested compressor is a semi-hermetic STC with the developed PWM inverter as the driver (Fig. 11 (b)). The compressor speed is regulated by this inverter, and the inverter output is the adjusted magnitude and frequency.

In order to verify the thermal balances of each component and the overall system, the pressures, temperatures, electrical powers, and flow rates were measured at the main locations of the test bench.

The test results are the power consumption, refrigerant flow rate, isentropic efficiency, and COP.

5. Results and discussion

5.1. Results of variable speed tests

This section discusses the tested performance of the developed STC with and without the ACM. The test conditions are listed in Table 1. The compressor operation frequency was set from 40 Hz to 80 Hz; the measured actual revolutions are also shown in Table 1.

Conditions A ~ E show the increase in operation speeds from 2261 rpm to 4612 rpm Fig. 12 (a) shows the test results of the compressor power consumption for the compressors with and without ACM. The power consumption was improved from 0.44% to 5.06%. Under the rating conditions (condition C), the compressor power consumption was approximately identical for both with and without ACM. Fig. 12 (b) shows that the overall COP increased from 0.61% to 13.5%. Under the rating condition (condition C), the compressor COP values were also nearly identical.

In Fig. 13, the growth rate of the noise level is not linear, and the point of condition D is a dividing point. However, the tests show

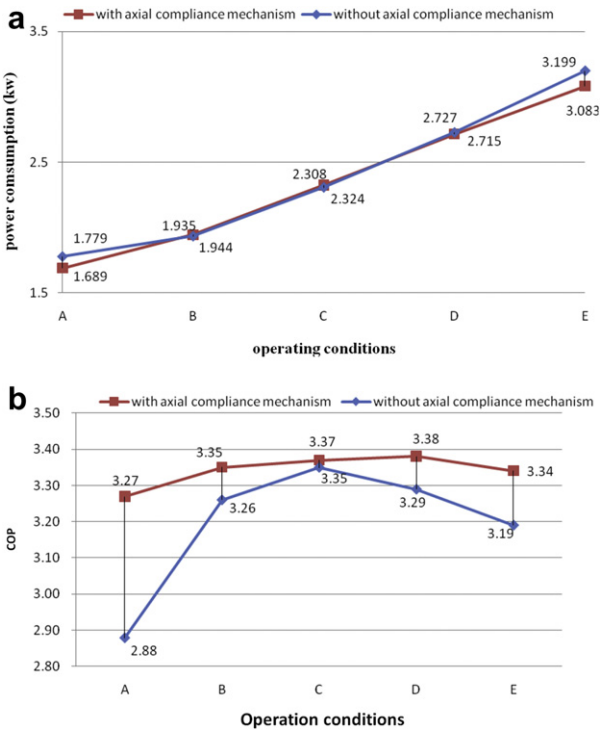

Fig. 12. Experiment results: (a) Power consumption vs. Operation speed (b) COP vs. Operation speed.

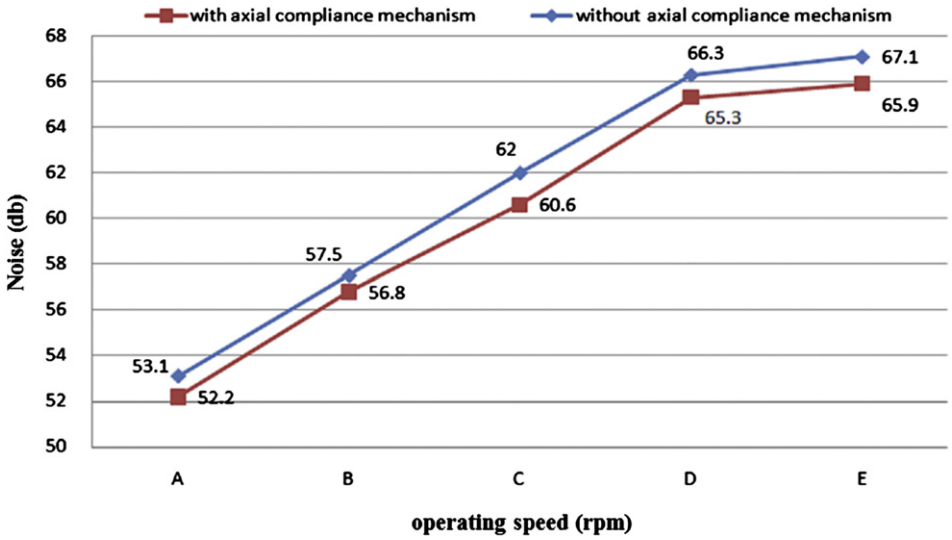

Fig. 13. Noise vs. Operation speed.

that the noise level was improved from 0.7 db to 1.4 db; further, the maximum noise level also improved (with and without ACM) by approximately 3%.

5.2. Discussion

Fig. 12 (a) and (b) imply that the ACM design can not only reduce the leakage loss (another say is increasing the cooling capacity) but also the frictional loss. Furthermore, from the slightly increasing trend, the rating condition can be considered suitable as a design base. The ACM function operates extremely well for clearance control and maintenance of high volumetric efficiency. The power consumption decreased from 0.44% to 5.06% but the overall COP increased from 0.61% to 13.53%. However, the cooling capacity increased from 0.91% to 7.79%.

The stiffness effect of the elastic element increases the ability to maintain the position of the fixed scroll while decreasing the tilting moment; further, the limiting ring maintains the position of the fixed scroll and reduces the degree of freedom of the scroll motion in the axial (vertical) direction.

In this manner, the ring limits the fixed scroll and makes it to move only along the axial direction. This reduces the contact opportunity and lowers the compressor noise lever. The ACM also reduces the high-frequency operation noise when the operating point is greater than that given under condition D. This is probably a result of mechanical structural improvements.

6. Conclusions

In this study, a suspension ACM with a limiting ring and two elastic elements (two crescent leaf springs) has been proposed for improving the STC performance. For the theoretical simulations of the leakage effect, a simplified leakage model was introduced in a numerical simulation package to improve the calculation time. The radial leakage could be precisely controlled within a preferred clearance distance. The performance test results of our STC prototype with the ACM design demonstrated that the proposed mechanism improves the COP at both higher and lower operation speeds. The conclusions are summarized as follows:

(1) Radial clearance (tip clearance) influences the leakage of scroll tips. Our simulation results show that the clearance should be less than 6 μm; this will ensure that the volume efficiency does not decrease with various operation speeds.
(2) The suspension ACM functions well at operation speeds from 4612 rpm (condition E) to 2261 rpm (condition A). The test results show the overall COP increases from 0.61% to 13.53%; moreover, these COP values were maintained about 3 even at higher and lower operation speeds due to the effective control of the radial clearance. Further, the power consumption was improved with the ACM design.
(3) The fixed ring structure constrained the fixed scroll and limited it to only axial direction movements. On the other hand, the back-pressure acting on the fixed scroll transferred its forces to frame via springs and caused a sufficient downward sealing force, leading to COP enhancement.
(4) Finally, the limiting ring prevented the scrolls from crashing, which led to reductions in the operating noise at extended operation speeds.

The effect of the ACM mechanism is based on the pressure difference between the suction pressure and discharge pressure. However, different refrigerants have different operating pressure differences. In this study, R22 refrigerant can be treated as the design base for other refrigerant applications. The future study may focus on R744 refrigerant for the much higher pressure difference.

In this manner, our ACM mechanism design improves the LPS STC performance at extended operation speeds.

Acknowledgement

The authors would like to express their gratitude for financial support from the Energy R&D foundation funding provided by the Energy Commission of the Ministry of Economic Affairs in Taiwan.

References

[1] T. Qureshi, S. Tassou, Variable speed capacity control in refrigeration Systems, Applied Thermal Engineering 16 (1996) 103–113.
[2] N. Ishii, M. Yamamura, H. Morokoshi, M. Fukushima, S. Yamamoto, M. Sakai, On the Superior dynamic behavior of a variable Rotating speed scroll compressor, in: Purdue International Compressor Engineering Conference Proceedings (1988), pp. 75–82.
[3] L. Hongqi, L. Quanping, W. Ruixiang, Research and Development of variable-speed scroll compressor, in: Purdue International Compressor Engineering Conference Proceedings (2002), pp. C24–C34.

[4] E. Morishita, M. Sugihara, T. Nakamura, Scroll compressor dynamics (1st report, the model for the fixed radius Crank), Bulletin of JSME 29 (248) (1986) 476–482.
[5] Baolong Wang, Xianting Li, Wenxing Shi, A general geometrical model of scroll compressors based on discretional initial angles of involute, International Journal of Refrigeration 28 (Issue 6) (September 2005) 958–966.
[6] K. Tojo, N. Ikegawa, N. Maeda, S. Machida, M. Shiibayashi, N. Uchikawa, Computer modeling of scroll compressor with self adjusting back pressure mechanism, in: Purdue International Compressor Engineering Conference Proceedings (1986), pp. 872–886.
[7] J.J. Nieter, Dynamics of suction process, in: Purdue International Compressor Engineering Conference Proceedings (1988), pp. 165–174.
[8] M. Hayano, H. Sakata, S. Nagatomo, H. Murasaki, An analysis of losses in scroll compressor, in: Purdue International Compressor Engineering Conference Proceedings (1988), pp. 189–197.
[9] H. Richardson, G. Gatecliff, Comparison of the high side vs. Low side Scroll Compressor design, in: Purdue International Compressor Engineering Conference Proceedings (1992), pp. 603–610.
[10] Joonhyun Lee, Seonkyo Kim, Seungkap Lee, Yoonser Park, Investigation of axial compliance mechanism in scroll compressor, in: Purdue International Compressor Engineering Conference Proceedings (1996), pp. 459–464.
[11] Youn Cheol Park, Yong chan Kim, Hong hyun Cho, Thermodynamic analysis on the performance of a variable speed scroll compressor with refrigerant Injection, International Journal of Refrigeration 25 (Issue 8) (December 2002) 1072–1082.
[12] Y.C. Chang, C.E. Tsai, C.H. Tseng, G.D. Tarng, L.T. Chang, Computer simulation and experimental Validation of scroll compressor, in: Purdue International Compressor Engineering Conference Proceedings (2004), p. C016.
[13] Y. Chen, N. Halm, J. Braun, E. Groll, Mathematical modeling of scroll compressor -part II: overall scroll compressor Modeling, International Journal of Refrigeration 25 (2002) 751–764.
[14] Nam-Kyu Cho, Young Youn, Byung-Chul Lee, Man-Ki Min, the characteristics of tangential leakage in scroll compressors for air-conditioners, in: , Purdue International Compressor Engineering Conference Proceedings, vol. I, 2000, pp. 807–814.
[15] Peter Howell, Fluid Mechanical Modeling of the Scroll Compressor, Mathematics for Science and Engineering. Cambridge University Press, Cambridge, UK, 2001, pp. 32–56.
[16] Li Liansheng, Scroll Compressors. Mechanical Industry. China, Beijing, 1998.
[17] C. Schein, R. Radermacher, Scroll compressor simulation model, Journal of Engineering for Gas Turbines and Power of ASME 123 (2001) 217–225.
[18] Young Youn, Nam-Kyu Cho, Byung-Chul Lee, Man-Ki Min, The characteristics of tip leakage in scroll compressors for air conditioners, in: , Purdue International Compressor Engineering Conference Proceedings, vol. I, 2000, pp. 797–805.
[19] T. Yanagisawa, T. Shimizu, Leakage losses with a rolling piston type Rotary compressor II - Leakage losses through clearances on rolling piston Faces, International Journal of Refrigeration 8 (no.3) (1985) 152–158.
[20] E.W. Lemmon, M.O. McLinden, M.L. Huber, REFPROP 8.0, NIST, MD, USA.
[21] Yuehju Tang, Chinghua Hung, Study of a Novel compliant suspension mechanism in low side type scroll compressor, in: Purdue International Compressor Engineering Conference Proceedings (2008), p. C1302.
[22] ASHRAE Method of Testing for Rating Positive Refrigerant Compressor and Condenser Uns. ASHRAE Standard ANSI/AHRAE-23, 1993.